



Robust fuzzy c-means clustering algorithm with adaptive spatial & intensity constraint and membership linking for noise image segmentation

Qingsheng Wang, Master's candidate, **Xiaopeng Wang**, Ph.D. *, **Chao Fang**, Ph.D.
Wenting Yang, Master's candidate

School of Electronic and Information Engineering, Lanzhou Jiaotong University, Lanzhou 730070, China



ARTICLE INFO

Article history:

Received 24 October 2019
 Received in revised form 5 March 2020
 Accepted 16 April 2020
 Available online 20 April 2020

Keywords:

FCM
 Noise image segmentation
 Local information
 Robustness

ABSTRACT

The fuzzy C-means (FCM) clustering method is proven to be an efficient method to segment images. However, the FCM method is not robust and less accurate for noise images. In this paper, a modified FCM method named FCM_SICM for noise image segmentation is proposed. Firstly, fast bilateral filter is used to acquire local spatial & intensity information; secondly, absolute difference image between the original image and the bilateral filtered image is employed and the reciprocal of the difference image and the difference image itself constrain conventional FCM as well as the local spatial & intensity information respectively; finally, membership linking is achieved by summing all membership degrees calculated from previous iteration within every cluster in squared logarithmic form as the denominator of objective function. Experiments show that this proposed method achieves superior segmentation performance in terms of segmentation accuracy (SA), average intersection-over-union (mIoU), E-measure and number of iteration steps on mixed noise images compared with several state-of-the-art methods.

© 2020 Elsevier B.V. All rights reserved.

1. Introduction

Image segmentation is an important process that partitions a digital image into several sets of pixels based on the similarities between pixels including luminance, color, texture, etc. to simplify the analysis of a given image. In the literature, there are various methods for image segmentation [1–4] and it is still a challenging task to design a robust and efficient segmentation method [5]. FCM [6,7] is an important unsupervised method that is not required to train image samples. It divides objects or patterns into several groups so that objects in the same group share similar characteristics while differ in different groups [8,9]. Although FCM clustering method is effective in segmentation for noise-free images, it has some drawbacks as it does not consider the local relationship between pixels and as a result it is sensitive to imaging noises and imaging artifacts [5].

Over the years, researchers have developed many FCM variants to reduce the noise sensitivity of conventional FCM method. In [5,10–25], FCM_S1/S2, FGFCM, HMRF_FCM, FLICM, KWFLICM, ARKFCM, Liu's method, RFCMLGI, IIFCM, GKWFPLICM, FLDNICM,

FRFCM, KBFWCM, SFFCM, RFCMSC, BCEFCM_S, APFFCM_S are presented. Methods described above are listed in time order. Except for FCM_S1/S2 [10] (it only incorporates local spatial information), they can be divided into five types based on different techniques besides local spatial information: (1) Histogram clustering including FGFCM [11], FRFCM [20] and SFFCM [22]; (2) Clustering using prior probability function including HMRF_FCM [12], Liu's method [15] and FLDNICM [19]; (3) Clustering using kernel method including KWFLICM [13], ARKFCM [14], GKWFPLICM [18], KBFWCM [21]; (4) clustering based on local intensity information: FLICM [5], RFCMLGI [16] and BCEFCM_S [24]. (5) clustering based on other theories including intuitionistic fuzzy set, rough set and entropy: IIFCM [17], RFCMSC [23] and APFFCM_S [25].

First of all, in histogram clustering, local information is considered before clustering and clustering speed is very fast, but there is no spatial information included in histogram clustering process. Secondly, although prior probability functions including hidden Markov random field are good tools to treat uncertainty, they are based on assumptions. Thirdly, kernel methods are designed to deal with non-linear classification problems. However, improvements are limited to some extent for noise image segmentation. Finally, FCM with local spatial and intensity information is efficient in light and single noise image segmentation, but original FCM is not constrained and there is no consideration for number of iteration steps.

* Corresponding author.

E-mail addresses: wqshmzh521@hotmail.com (Q. Wang), wangxiaopeng@mail.lzjtu.cn (X. Wang), fangchao@mail.lzjtu.cn (C. Fang), 1540116397@qq.com (W. Yang).

In general, the number of clusters varies among people. For image segmentation, the number of significant peaks in image histogram is often considered as reference for automatic cluster number selection [26]. But for noise image, on the one hand, each bar in histogram is intended to be equalized because of noise and therefore peaks are hard to identify; on the other hand, many noise pixels (outliers) exist and thus methods in [27–30] cannot work well. Since the number of clusters may not be determined in single approach or before performing clustering, other ways are possible. Different cluster validity indexes, including sum of within-cluster distances, sum of within-cluster square error, CH index [31], KL index [32], Silhouette index [33] and so on, can be used through numerous approaches on a series of possible number of clusters to automatically select a proper number of clusters. For the sum of within-cluster distances, or the sum of within-cluster square error, the proper number of clusters comes when the first index is small, or when the decreasing speed of the second index changes the most (elbow point). For CH, KL and Silhouette indexes, proper number of clusters is presented when they reach the maximum value. In [34], “gap statistic” method is proposed to determine the number of clusters. This method computes the difference of the sum of within-cluster distances between observed data and reference data, which is sampled by Monte Carlo method, in logarithmic form. However, only when the observed data is close to be uniformly distributed can “gap statistic” method selects a proper number of clusters. In practice, proper number of clusters can be automatically selected via numerous approaches according to different cluster validity indexes.

In this paper, we propose an improved FCM with adaptive spatial & intensity constraint and membership linking (FCM_SICM) for noise image segmentation. In FCM_SICM, firstly, fast bilateral filter is used to acquire the local spatial & intensity information of the image; secondly, by considering absolute difference between original image and spatial & intensity information, not only the local spatial & intensity information, but also the original FCM are constrained in a simple and adaptive way; thirdly, in order to reduce iteration steps, membership linking is proposed by adding all membership degrees within each cluster calculated in previous iteration in squared logarithmic form and by considering it as denominator of objective function. There are three main characteristics of FCM_SICM: (1) Constraints of spatial & intensity and original FCM are adaptively specified and vary between pixels. (2) Membership linking is proposed to reduce iteration steps; (3) Segmentation quality of mixed noise images is better than that of state-of-the-art methods.

The remaining parts of this paper are organized as follows. In Section 2, the fast bilateral filter and conventional FCM are introduced. In Section 3, motivations are introduced. In Section 4, the FCM_SICM is presented. In Section 5, several experiments are implemented. In Section 6, discussion is provided and conclusion is drawn in Section 7.

2. Preliminary theory

2.1. Fast bilateral filtering method

Conventional spatial filters, such as Gaussian filter, are achieved by only taking relationships of spatial coordinates between pixels in neighborhood of a center pixel into account and therefore smooth the inhomogeneous regions and image edges simultaneously. In [35], a novel filter called bilateral filter that considers not only the relationships of spatial locations but also intensity between pixels and consequently preserves image details like edges. The equations of which are given as:

$$\omega(i, j, k, l) = \exp \left[-\frac{(i-k)^2 + (j-l)^2}{2\sigma_d^2} - \frac{\|I(i, j) - I(k, l)\|^2}{2\sigma_r^2} \right] \quad (1)$$

$$I_D(i, j) = \frac{\sum_{k,l} I(k, l) \omega(i, j, k, l)}{\sum_{k,l} \omega(i, j, k, l)} \quad (2)$$

where σ_d and σ_r are geometric spread and photometric spread respectively, $I_D(i, j)$ is the result of bilateral filtering, $I(i, j)$ and $I(k, l)$ are pixel values of the pixel (i, j) and (k, l) respectively, (k, l) is a pixel in the neighborhood whose center pixel is (i, j) . It can be seen that the computational complexity of Eq. (2) is $O(n^4)$ and thus requires plenty of average running time to filter a given image.

For solving this problem, in [36], a fast approximation method using signal processing approach is proposed to accelerate the conventional bilateral filter. This method is achieved by expressing the filter formula in a higher dimension where pixel intensity is added to the original dimensions and thus the formula is written as simple linear convolutions after the original image is downsampled. Finally, the convolution result is upsampled and division is operated only once [36]. The formulas of this proposed method are given as:

$$\begin{pmatrix} w_p^{bf} & i_p^{bf} \\ w_p^{bf} & i_p^{bf} \end{pmatrix} = \sum_{q \in S} \sum_{\zeta \in R} G_{\sigma_d}(\|p - q\|) G_{\sigma_r}(|i_p - \zeta|) \delta(\zeta - i_q) \begin{pmatrix} w_q i_q \\ w_q \end{pmatrix} \quad (3)$$

$$I_p^{bf} = \frac{w_p^{bf} i_p^{bf}}{w_p^{bf}} \quad (4)$$

where $\delta(\zeta - i_q)$ (1 if $\zeta = i_q$, 0 otherwise) is Kronecker symbol defines on \mathbb{R} , p is the coordinate of a pixels in a neighborhood, i_q is the luminance of the pixel q , q is the coordinate of the neighborhood's center, i_p is the luminance of the neighborhood pixel p , R is the image grayscale level domain, S is the 2D spatial coordinates (x, y) of whole image domain, w_q is a 3D point whose coordinate is (x, y, ζ) and $w_q = 1$ if (x, y, ζ) is (x, y, i_q) and $w_q = 0$ otherwise, $w_q i_q$ is a 3D point whose coordinate is the same as w_q 's but differs in the value that it is either i_q when (x, y, ζ) is (x, y, i_q) or 0 when otherwise.

In order to accelerate, $w_q i_q$ and w_q are downsampled to become w_{\downarrow} and w_{\downarrow} by average downsampling and then w_{\downarrow} and w_{\downarrow} are applied into Eq. (1) to get $w_{\downarrow}^{bf} i_{\downarrow}^{bf}$ and w_{\downarrow}^{bf} . Then, $w_{\downarrow}^{bf} i_{\downarrow}^{bf}$ and w_{\downarrow}^{bf} are upsampled by linear interpolation to get $w_{\uparrow\downarrow}^{bf} i_{\uparrow\downarrow}^{bf}$ and $w_{\uparrow\downarrow}^{bf}$. Finally, $w_{\uparrow\downarrow}^{bf} i_{\uparrow\downarrow}^{bf}$ and $w_{\uparrow\downarrow}^{bf}$ are applied into Eq. (2) to get the final bilateral filtered pixel I_p^{bf} .

Algorithm 1. Fast bilateral filtering proposed in [36].

Input: Original image I , geometric spread σ_d , photometric spread σ_r .

1. Create 3D matrix W and WI
2. Downsample W and WI using average downsampling with $(2\sigma_d + 1) \times (2\sigma_d + 1) \times (2\sigma_r + 1)$ neighborhood to get W_{\downarrow} and $W_{\downarrow} I_{\downarrow}$.
3. Apply W_{\downarrow} and $W_{\downarrow} I_{\downarrow}$ into Eq. (3) to find W_{\downarrow}^{bf} and $W_{\downarrow}^{bf} I_{\downarrow}^{bf}$.
4. Upsample W_{\downarrow}^{bf} and $W_{\downarrow}^{bf} I_{\downarrow}^{bf}$ using linear interpolation to find $W_{\uparrow\downarrow}^{bf}$ and $W_{\uparrow\downarrow}^{bf} I_{\uparrow\downarrow}^{bf}$.
5. Apply $W_{\uparrow\downarrow}^{bf}$ and $W_{\uparrow\downarrow}^{bf} I_{\uparrow\downarrow}^{bf}$ into Eq. (4).
6. **Return** The bilateral filtered result I_p^{bf} .

2.2. FCM clustering method

The FCM clustering method is firstly given in [37] and then extended in [38]. This method is achieved by updating the objective function $J_{FCM}^{(a)}$ to convergence through several iterations to

partition data vectors into optimal clusters. The objective function $J_{FCM}^{(a)}$ is given as:

$$J_{FCM}^{(a)} = \sum_{i=1}^K \sum_{j=1}^N (u_{ij}^{(a)})^m \|y_j - c_i^{(a)}\|^2, \quad \sum_{i=1}^K u_{ij}^{(a)} = 1 \quad (5)$$

where y_j is the j th pixel in image I , N is the total number of pixels, K is the number of clusters, $u_{ij}^{(a)}$ is the membership degree of y_j to i th cluster in a th iteration (a is surrounded by brackets in order not to be misidentified as power operator), m is the weighting exponent on $u_{ij}^{(a)}$ and usually equals to two, $c_i^{(a)}$ is the prototype of the cluster center of i th cluster in a th iteration.

By Lagrangian multiplier method, Eq. (5) is minimized by updating the follows:

$$u_{ij}^{(a)} = \frac{1}{\sum_{r=1}^K \left(\frac{\|y_j - c_r^{(a)}\|}{\|y_j - c_r^{(a)}\|} \right)^{\frac{2}{m-1}}} \quad (6)$$

$$c_i^{(a)} = \frac{\sum_{j=1}^N (u_{ij}^{(a)})^m y_j}{\sum_{j=1}^N (u_{ij}^{(a)})^m} \quad (7)$$

Algorithm 2. FCM method

Input: Set number of clusters K , weighting exponent on membership degree m , minimum error ε .

1. Set all center vectors $c_i^{(0)}$ to 0.
2. Randomly initialize all membership degrees $u_{ij}^{(0)}$.
3. Set loop counter $a = 1$.
4. **Repeat**
 - a. Update center vectors $c_i^{(a)}$ by Eq. (7).
 - b. Update membership degrees $u_{ij}^{(a)}$ by Eq. (6).
 - c. Update objective function $J_{FCM}^{(a)}$ by Eq. (5).
 - d. $a = a + 1$.
5. **Until** $\|J_{FCM}^{(a)} - J_{FCM}^{(a-1)}\| < \varepsilon$, $a > 1$.
6. **Return** Membership degrees $u_{ij}^{(a)}$
7. Apply each data point into the cluster whose membership degree is the highest.

3. Motivations

3.1. Motivation of using local spatial & intensity information

For the purpose of enhancing the denoising performance of FCM, many FCM variants have been proposed. Generally, the objective function regularized by local information is given as:

$$J^{(a)} = \sum_{i=1}^K \sum_{j=1}^N (u_{ij}^{(a)})^m \|y_j - c_i^{(a)}\|^2 + \sum_{i=1}^K \sum_{j=1}^N G_{ij}^{(a)} \quad (8)$$

where $G_{ij}^{(a)}$ is the j th fuzzy factor within i th cluster during a th iteration. For FCM_S1/S2, only spatial information is utilized and therefore inhomogeneous regions and image edges are equally smoothed. Proved by FGFCM, FLICM, KWFLICM, RFCMLGI and GKWFLICM, local spatial and intensity information is able to preserve image edges. For HMRF_FCM, FLICM, KWFLICM, Liu's method, IIFCM, GKWFLICM, FLDNICM, KBFWCM, BCEFCM_S and APFCM_S, the computational overloads are $O(n^4)$ individually. Therefore, in order to reduce complexity and maintain or increase segmentation quality, simple structure of formula is required.

In practice, we consider to acquire a method that incorporates local spatial and intensity information before clustering to reduce computational overload. Motivated by this, we choose the

fast bilateral filtering method and the objective function of the proposed method is given as:

$$\begin{aligned} J_{FCM_SICM}^{(a)} = & \sum_{i=1}^K \sum_{j=1}^N \alpha(u_{ij}^{(a)})^m \|y_j - c_i^{(a)}\|^2 \\ & + \sum_{i=1}^K \sum_{j=1}^N \beta(u_{ij}^{(a)})^m \|\bar{y}_j - c_i^{(a)}\|^2 \end{aligned} \quad (9)$$

where α and β are the constraints of original image and fast bilateral filtered image, \bar{y}_j is the j th pixel in the fast bilateral filtered image. In this way, the computational complexity is reduced to $O(n^3)$ and not only spatial and intensity information but also the original FCM, are constrained.

3.2. Motivation of using membership linking

In FCM, for the purpose of minimizing the objective function, we utilize Lagrange multiplier method to derive the formulas to update the membership degrees and clustering centers and in the end the objective function is able to be minimized anyway. However, the number of iteration steps is not considered in many cases.

It is discovered that for i th cluster, the sum of memberships degrees computed from previous iteration can be used to reduce the number of iteration steps and it is called membership linking M :

$$M = \sum_{e=1}^N u_{ie}^{(a-1)} \quad (10)$$

In this paper, M is considered as the denominator of Eq. (9) as:

$$\begin{aligned} J_{FCM_SICM}^{(a)} &= \sum_{i=1}^K \frac{\sum_{j=1}^N \alpha(u_{ij}^{(a)})^m \|y_j - c_i^{(a)}\|^2 + \sum_{j=1}^N \beta(u_{ij}^{(a)})^m \|\bar{y}_j - c_i^{(a)}\|^2}{\sum_{e=1}^N u_{ie}^{(a-1)}} \end{aligned} \quad (11)$$

For a given image, the larger the image size, the larger the sum of memberships of all the pixels, i.e. the larger the Eq. (10). In order to avoid the situations where the objective function reaches convergence so early before the method outputs a satisfied result, M is modified into logarithmic form:

$$M = \ln(\sum_{e=1}^N u_{ie}^{(a-1)} + 1) \quad (12)$$

According to the trends of logarithmic function, M is able to be reduced into a smaller number. However, when Eq. (10) is large, for different clusters, Eq. (12) changes very little and it is difficult to distinguish different clusters. Therefore, M is modified as:

$$M = \ln^2(\sum_{e=1}^N u_{ie}^{(a-1)} + 1) \quad (13)$$

Accordingly, Eq. (11) is then modified as:

$$\begin{aligned} J_{FCM_SICM}^{(a)} &= \sum_{i=1}^K \frac{\sum_{j=1}^N \alpha(u_{ij}^{(a)})^m \|y_j - c_i^{(a)}\|^2 + \sum_{j=1}^N \beta(u_{ij}^{(a)})^m \|\bar{y}_j - c_i^{(a)}\|^2}{\ln^2(\sum_{e=1}^N u_{ie}^{(a-1)} + 1)} \end{aligned} \quad (14)$$

4. Proposed method: robust fuzzy c-means with adaptive spatial & intensity constraint and membership linking (FCM_SICM)

Conventional FCM is proven to be a method sensitive to noise and therefore it is hard to segment noisy images. We propose an improved FCM that incorporates local spatial & intensity information and membership linking for noise image segmentation.

The objective function $J_{FCM_SICM}^{(a)}$ of this proposed method is firstly given as:

$$\begin{aligned} J_{FCM_SICM}^{(a)} \\ = \sum_{i=1}^K \frac{\sum_{j=1}^N \alpha(u_{ij}^{(a)})^m \|y_j - c_i^{(a)}\|^2 + \sum_{j=1}^N \beta(u_{ij}^{(a)})^m \|\bar{y}_j - c_i^{(a)}\|^2}{\ln^2(\sum_{e=1}^N u_{ie}^{(a-1)} + 1)} \end{aligned} \quad (15)$$

It is necessary to consider how to select proper α and β . When noise is heavier, it is necessary to select a smaller α and a larger β . By doing this, the segmentation result can be better influenced by the bilateral filtered image while original image is preserved to a certain extent. In practice, different α and β are needed to be applied for segmenting different images. Also, α and β are fixed for all pixels i.e. tradeoffs between pixels in original image and bilateral filtered image are the same. Therefore, the proposed method is not flexible by applying α and β .

For a noisy image, the more seriously is pixel y_j corrupted by noise, the larger is the $|y_j - \bar{y}_j|$ i.e. the intensity difference between the original pixel and the bilateral filtered pixel is larger. That is, the segmentation result is supposed to be better influenced by the bilateral filtered image (a larger β is needed) and less influenced by the original image (a smaller α is needed). Here, $|y_j - \bar{y}_j|$ and $1/|y_j - \bar{y}_j|$ are used to measure the extent of influence of bilateral filtered image and the original image on segmentation result respectively:

$$\beta = |y_j - \bar{y}_j| \quad (16)$$

$$\alpha = \frac{1}{|y_j - \bar{y}_j|} \quad (17)$$

By applying Eqs. (16) and (17), each pixel has its own tradeoff between the original image and the bilateral filtered image and manual selection of α and β is not required anymore.

It has been proved in practice that replacing β and α with Eqs. (16) and (17) is not enough for the proposed method to output a satisfied segmentation result. It is discovered that only by increasing $|y_j - \bar{y}_j|$ can a better quality segmentation result be obtained. After several experiments, it is discovered that timing $|y_j - \bar{y}_j|$ by 20 is suitable enough. Meanwhile, for the prevention of Inf and zero, a small number eps is added to Eqs. (16) and (17). Consequently, Eqs. (16) and (17) are modified as:

$$\beta = 20 |y_j - \bar{y}_j| + eps \quad (18)$$

$$\alpha = \frac{1}{20 |y_j - \bar{y}_j| + eps} \quad (19)$$

By applying Eqs. (18) and (19) into Eq. (15), the objective function $J_{FCM_SICM}^{(a)}$ is modified as Eq. (20) given in Box I.

Considering that $|y_j - \bar{y}_j|$ is related with only pixels in original image and bilateral filtered image and does not change during iterations, $|y_j - \bar{y}_j|$ can be computed only once before iterations. Let

$$\Delta I = 20 |I - \bar{I}| + eps \quad (21)$$

where I is the original image, \bar{I} is the bilateral filtered image. ΔI is the difference between I and \bar{I} . The objective function $J_{FCM_SICM}^{(a)}$ is finally given as:

$$J_{FCM_SICM}^{(a)}$$

$$\begin{aligned} &= \sum_{i=1}^K \frac{\sum_{j=1}^N \frac{1}{\Delta y_j} (u_{ij}^{(a)})^m \|y_j - c_i^{(a)}\|^2 + \sum_{j=1}^N \Delta y_j (u_{ij}^{(a)})^m \|\bar{y}_j - c_i^{(a)}\|^2}{\ln^2(\sum_{e=1}^N u_{ie}^{(a-1)} + 1)}, \\ &\sum_{i=1}^K u_{ij}^{(a)} = 1 \end{aligned} \quad (22)$$

where Δy_j is the j th value of ΔI .

Theorem 1. Using Lagrange multiplier method, Lagrange function F is given as:

$$\begin{aligned} F = \sum_{i=1}^K \frac{\sum_{j=1}^N \frac{1}{\Delta y_j} (u_{ij}^{(a)})^m \|y_j - c_i^{(a)}\|^2 + \sum_{j=1}^N \Delta y_j (u_{ij}^{(a)})^m \|\bar{y}_j - c_i^{(a)}\|^2}{\ln^2(\sum_{e=1}^N u_{ie}^{(a-1)} + 1)} \\ + \sum_{j=1}^N \lambda_j (1 - \sum_{i=1}^K u_{ij}^{(a)}) \end{aligned} \quad (23)$$

where λ_j is Lagrange multiplier.

Take the partial derivative of Eq. (23) with respect to $u_{ij}^{(a)}$, $c_i^{(a)}$ and λ_j respectively and let them equal to 0, then $u_{ij}^{(a)}$ and $c_i^{(a)}$ can be derived as:

$$u_{ij}^{(a)} = \frac{1}{\sum_{r=1}^K \left[\frac{\frac{1}{\Delta y_j} \|y_j - c_i^{(a)}\|^2 + \Delta y_j \|\bar{y}_j - c_i^{(a)}\|^2}{\ln^2(\sum_{e=1}^N u_{ie}^{(a-1)} + 1)} \right]^{\frac{1}{m-1}}} \quad (24)$$

$$c_i^{(a)} = \frac{\sum_{j=1}^N \left(\frac{1}{\Delta y_j} y_j + \Delta y_j \bar{y}_j \right) (u_{ij}^{(a)})^m}{\sum_{j=1}^N \left(\frac{1 + \Delta y_j^2}{\Delta y_j} \right) (u_{ij}^{(a)})^m} \quad (25)$$

Proof. The minimization of the Eq. (22) is equivalent to the minimization of the Eq. (23). Take the partial derivative of Eq. (23) with respect to membership degree $u_{ij}^{(a)}$, and λ_j and let them equal to zero:

$$\frac{\partial F}{\partial u_{ij}^{(a)}} = 0$$

$$\Rightarrow \frac{m(u_{ij}^{(a)})^{m-1} \frac{1}{\Delta y_j} \|y_j - c_i^{(a)}\|^2 + m(u_{ij}^{(a)})^{m-1} \Delta y_j \|\bar{y}_j - c_i^{(a)}\|^2}{\ln^2(\sum_{e=1}^N u_{ie}^{(a-1)} + 1)} - \lambda_j = 0$$

$$\Rightarrow \frac{m(u_{ij}^{(a)})^{m-1} \frac{1}{\Delta y_j} \|y_j - c_i^{(a)}\|^2 + m(u_{ij}^{(a)})^{m-1} \Delta y_j \|\bar{y}_j - c_i^{(a)}\|^2}{\ln^2(\sum_{e=1}^N u_{ie}^{(a-1)} + 1)} = \lambda_j$$

$$\Rightarrow u_{ij}^{(a)} = \left[\frac{\lambda_j \ln^2(\sum_{e=1}^N u_{ie}^{(a-1)} + 1)}{m \frac{1}{\Delta y_j} \|y_j - c_i^{(a)}\|^2 + m \Delta y_j \|\bar{y}_j - c_i^{(a)}\|^2} \right]^{\frac{1}{m-1}} \quad (26)$$

$$\Rightarrow u_{ij}^{(a)} = \left(\frac{\lambda_j}{m} \right)^{\frac{1}{m-1}} \frac{1}{\left[\frac{\frac{1}{\Delta y_j} \|y_j - c_i^{(a)}\|^2 + \Delta y_j \|\bar{y}_j - c_i^{(a)}\|^2}{\ln^2(\sum_{e=1}^N u_{ie}^{(a-1)} + 1)} \right]^{\frac{1}{m-1}}} \quad (26)$$

$$\frac{\partial F}{\partial \lambda_j} = 0 \Rightarrow \sum_{i=1}^K u_{ij}^{(a)} = 1 \quad (27)$$

$$J_{FCM_SICM}^{(a)} = \sum_{i=1}^K \frac{\sum_{j=1}^N \frac{1}{20|y_j - \bar{y}_j| + eps} (u_{ij}^{(a)})^m \|y_j - c_i^{(a)}\|^2 + \sum_{j=1}^N (20|y_j - \bar{y}_j| + eps) (u_{ij}^{(a)})^m \|\bar{y}_j - c_i^{(a)}\|^2}{\ln^2(\sum_{e=1}^N u_{ie}^{(a-1)} + 1)}, \sum_{i=1}^K u_{ij}^{(a)} = 1 \quad (20)$$

Box I.

Substitute Eq. (26) into Eq. (27):

$$\begin{aligned} \sum_{i=1}^K u_{ij}^{(a)} &= \left(\frac{\lambda_j}{m}\right)^{\frac{1}{m-1}} \sum_{i=1}^K \frac{1}{\left[\frac{\frac{1}{\Delta y_j} \|y_j - c_i^{(a)}\|^2 + \Delta y_j \|\bar{y}_j - c_i^{(a)}\|^2}{\ln^2(\sum_{e=1}^N u_{ie}^{(a-1)} + 1)}\right]^{\frac{1}{m-1}}} = 1 \\ &\Rightarrow \left(\frac{\lambda_j}{m}\right)^{\frac{1}{m-1}} = \frac{1}{\sum_{i=1}^K \left[\frac{\frac{1}{\Delta y_j} \|y_j - c_i^{(a)}\|^2 + \Delta y_j \|\bar{y}_j - c_i^{(a)}\|^2}{\ln^2(\sum_{e=1}^N u_{ie}^{(a-1)} + 1)}\right]^{\frac{1}{m-1}}} \end{aligned} \quad (28)$$

Substitute Eq. (28) into Eq. (26):

$$\begin{aligned} u_{ij}^{(a)} &= \frac{1}{\sum_{r=1}^K \left[\frac{1}{\left[\frac{\frac{1}{\Delta y_j} \|y_j - c_r^{(a)}\|^2 + \Delta y_j \|\bar{y}_j - c_r^{(a)}\|^2}{\ln^2(\sum_{e=1}^N u_{re}^{(a-1)} + 1)}\right]^{\frac{1}{m-1}}} - \left[\frac{\frac{1}{\Delta y_j} \|y_j - c_i^{(a)}\|^2 + \Delta y_j \|\bar{y}_j - c_i^{(a)}\|^2}{\ln^2(\sum_{e=1}^N u_{ie}^{(a-1)} + 1)}\right]^{\frac{1}{m-1}}\right]} \\ &\Rightarrow u_{ij}^{(a)} = \frac{1}{\sum_{r=1}^K \left[\frac{\frac{1}{\Delta y_j} \|y_j - c_r^{(a)}\|^2 + \Delta y_j \|\bar{y}_j - c_r^{(a)}\|^2}{\ln^2(\sum_{e=1}^N u_{re}^{(a-1)} + 1)}\right]^{\frac{1}{m-1}} - \left[\frac{\frac{1}{\Delta y_j} \|y_j - c_i^{(a)}\|^2 + \Delta y_j \|\bar{y}_j - c_i^{(a)}\|^2}{\ln^2(\sum_{e=1}^N u_{ie}^{(a-1)} + 1)}\right]^{\frac{1}{m-1}}} \end{aligned}$$

Take the partial derivative of Eq. (23) with respect to cluster center $c_i^{(a)}$ and let it equal to zero:

$$\begin{aligned} \frac{\partial F}{\partial c_i^{(a)}} &= 0 \\ &\Rightarrow -2 \sum_{j=1}^N \frac{1}{\Delta y_j} (u_{ij}^{(a)})^m \|y_j - c_i^{(a)}\| - 2 \sum_{j=1}^N \Delta y_j (u_{ij}^{(a)})^m \|\bar{y}_j - c_i^{(a)}\| = 0 \\ &\Rightarrow \sum_{j=1}^N (u_{ij}^{(a)})^m \frac{1}{\Delta y_j} y_j - \sum_{j=1}^N (u_{ij}^{(a)})^m \frac{1}{\Delta y_j} c_i^{(a)} + \sum_{j=1}^N (u_{ij}^{(a)})^m \Delta y_j \bar{y}_j \\ &\quad - \sum_{j=1}^N (u_{ij}^{(a)})^m \Delta y_j c_i^{(a)} = 0 \\ &\Rightarrow \sum_{j=1}^N (u_{ij}^{(a)})^m \left(\frac{y_j}{\Delta y_j} + \Delta y_j \bar{y}_j\right) = c_i^{(a)} \sum_{j=1}^N (u_{ij}^{(a)})^m \left(\frac{1}{\Delta y_j} + \Delta y_j\right) \\ &\Rightarrow c_i^{(a)} = \frac{\sum_{j=1}^N \left(\frac{1}{\Delta y_j} y_j + \Delta y_j \bar{y}_j\right) (u_{ij}^{(a)})^m}{\sum_{j=1}^N \left(\frac{1+\Delta y_j^2}{\Delta y_j}\right) (u_{ij}^{(a)})^m} \end{aligned}$$

This completes the proof.

By updating $u_{ij}^{(a)}$ and $c_i^{(a)}$ using Eqs. (24) and (25) respectively, the objective function can be minimized. Then, the proposed

method outputs optimal membership degrees $u_{ij}^{(a)}$. Finally, apply each pixel to the cluster whose membership degree is the highest.

Method 3. FCM_SICM method

Input: Set number of clusters K , weighting exponent on membership degree m , minimum error ε , small number $eps = 0.000001$, geometric spread σ_d and photometric spread σ_r .

1. Normalize the original image into $[0, 1]$.
2. Filter the original image using fast bilateral filter proposed in [35] with σ_d and σ_r specified in manual.
3. Find the difference image ΔI between original image and bilateral filtered image.
4. Set center vectors $c_i^{(1)}$ to 0.
5. Randomly initialize all membership degrees $u_{ij}^{(1)}$.
6. Set $u_{ij}^{(0)} = u_{ij}^{(1)}$ to compute membership linking in the first iteration.
7. Set loop counter $a = 1$.
8. Repeat
 - a. Update center vectors $c_i^{(a)}$ using Eq. (25).
 - b. Update membership degrees $u_{ij}^{(a)}$ using equation Eq. (24).
 - c. Update objective function $J_{FCM_SICM}^{(a)}$ using Eq. (22).
 - d. $a = a + 1$.
9. Until $\|J_{FCM_SICM}^{(a)} - J_{FCM_SICM}^{(a-1)}\| < \varepsilon, a > 1$.
10. **Return** Membership degrees $u_{ij}^{(a)}$.
11. Apply each pixel into the cluster whose membership degree is the highest.

5. Experiments

5.1. The motivation and the way to add mixed noise

In other papers presenting state-of-the-art methods [5,10–25], only one type or two types of additive noise is added to the test images and these methods are well performed. In this paper, in order to test methods in a real-like environment, mixed noise is added to all the test images.

In this section, the mixed noise is constructed by three kinds of noise: Gaussian noise, salt & pepper noise and uniformly distributed multiplicative noise. The way to add mixed noise is given as follows:

- Step 1: Specify a number d .
- Step 2: Convert the data type of image I into “double” and normalize I into $[0, 1]$.
- Step 3: Add Gaussian noise with zero mean and d variance to image I .
- Step 4: Add salt & pepper noise with density of d to image I .
- Step 5: Add uniformly distributed multiplicative noise with zero mean and d variance to image I .
- Step 6: Normalize image I into $[0, 255]$ and convert the data type to “uint8”.

In the experiments followed, the mixed noise is described as “100*d% mixed noise”

5.2. Experiment settings

Experimental results of the proposed method are shown by presenting results on real and synthetic images. The test CPU

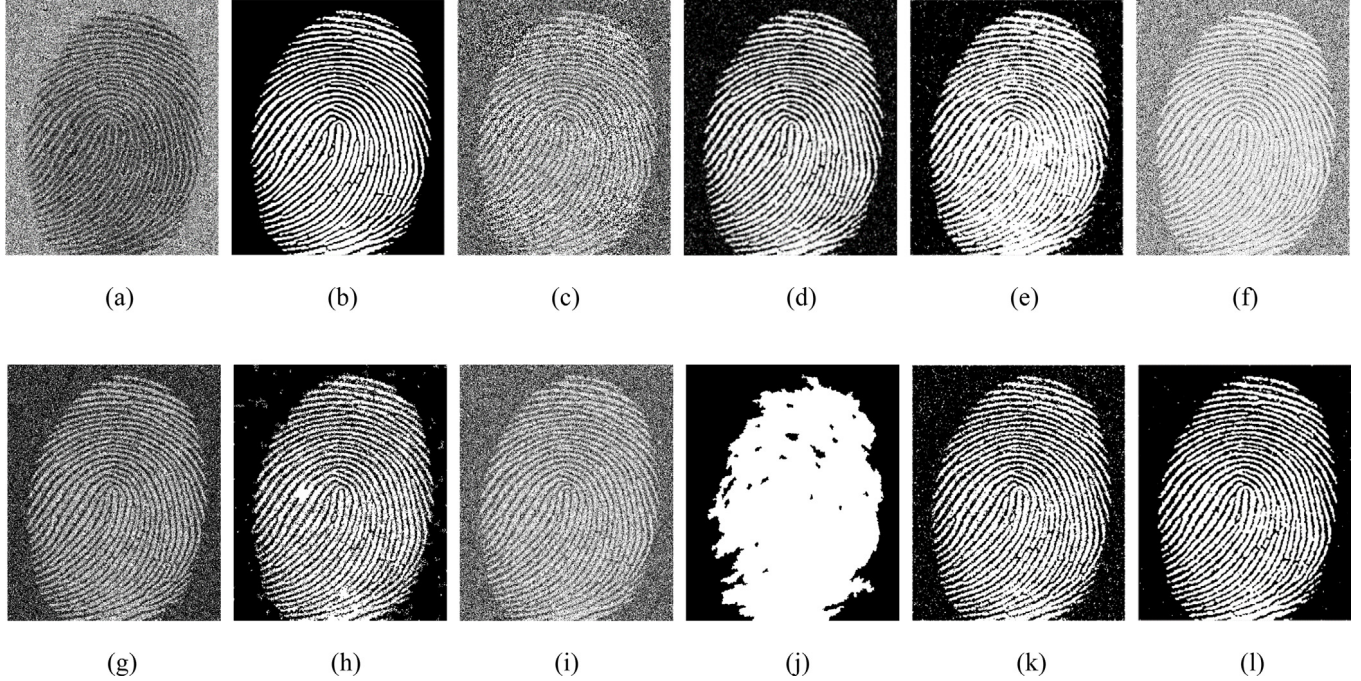


Fig. 1. Segmentation results on fingerprint image corrupted by 15% mixed noise using different methods. (a) Original image corrupted by 15% mixed noise. (b) Ground-truth. (c) FCM result. (d) FGFCM result with $\lambda_s = 3$ and $\lambda_g = 5$. (e) FLICM result. (f) ARKFCM result. (g) IIFCM result with $\lambda = 1.5$. (h) FRFCM result. (i) FLDNICM result. (j) SFFCM result. (k) APFCM_S result with $p = 3$, $q = 6$, $\alpha = 0.6$ and $\lambda = 10^7$. (l) FCM_SICM result with $\sigma_d = 2.5$ and $\sigma_r = 5$.

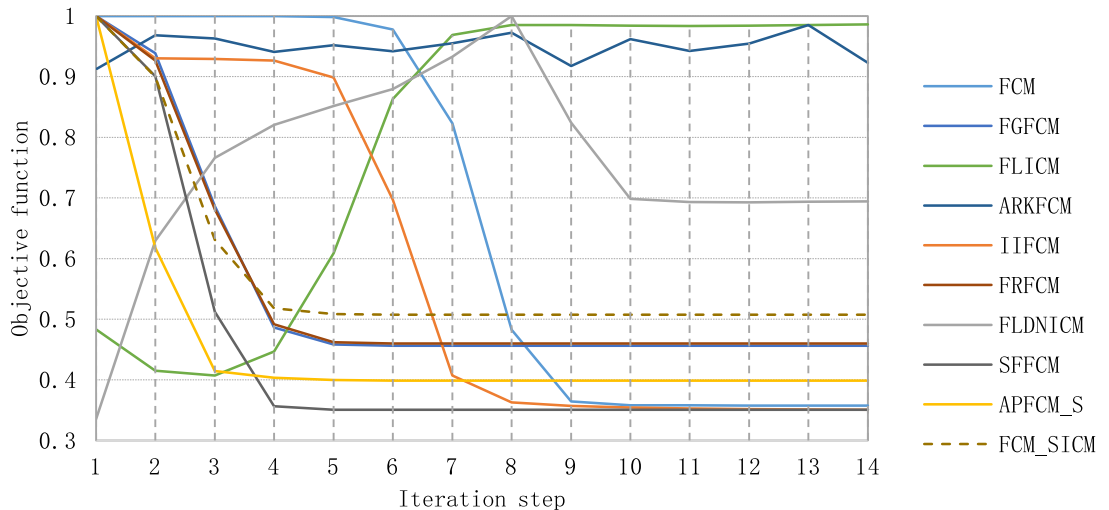


Fig. 2. Graph of objective function curves that normalized into $[0, 1]$ of ten methods for Fig. 1.

is Intel i7-4710HQ. The experimental results of FCM_SICM are compared with FCM, FGFCM, FLICM, ARKFCM, IIFCM, FRFCM, FLDNICM, SFFCM, APFCM_S. All experimenting images are corrupted by 1%, 5%, 10%, 15% and 20% mixed noise, respectively. All the experimental results are performed with respect of segmentation accuracy (SA), average intersection-over-union (mIoU), objective function curves graph, number of iteration steps and additionally E-Measure proposed in [39] for binary image segmentation.

Segmentation accuracy (SA) is defined as the proportion of the sum of correctly clustered pixels to the sum of all pixels:

$$SA = \frac{\sum_{i=1}^K A_i \cap C_i}{\sum_{j=1}^K C_j} \quad (29)$$

where A_i is the set of pixels in i th cluster found by the method, C_i is the set of pixels in i th cluster in the ground-truth, and the larger

the SA, the better the result is. Average intersection-over-union (mIoU) is defined as:

$$mIoU = \frac{1}{K} \sum_{i=1}^K \frac{A_i \cap C_i}{A_i \cup C_i} \quad (30)$$

where all the symbols are the same as that of SA. It indicates the equality between the segmented image and the ground-truth. The larger the mIoU, the better the result is. E-Measure E is defined as:

$$E = \frac{1}{4mn} \sum_{x=1}^m \sum_{y=1}^n \left\{ 1 + \frac{2[I_{GT}(x, y) - \mu_{GT}][I_{FM}(x, y) - \mu_{FM}]}{[I_{GT}(x, y) - \mu_{GT}]^2 + [I_{FM}(x, y) - \mu_{FM}]^2} \right\}^2 \quad (31)$$

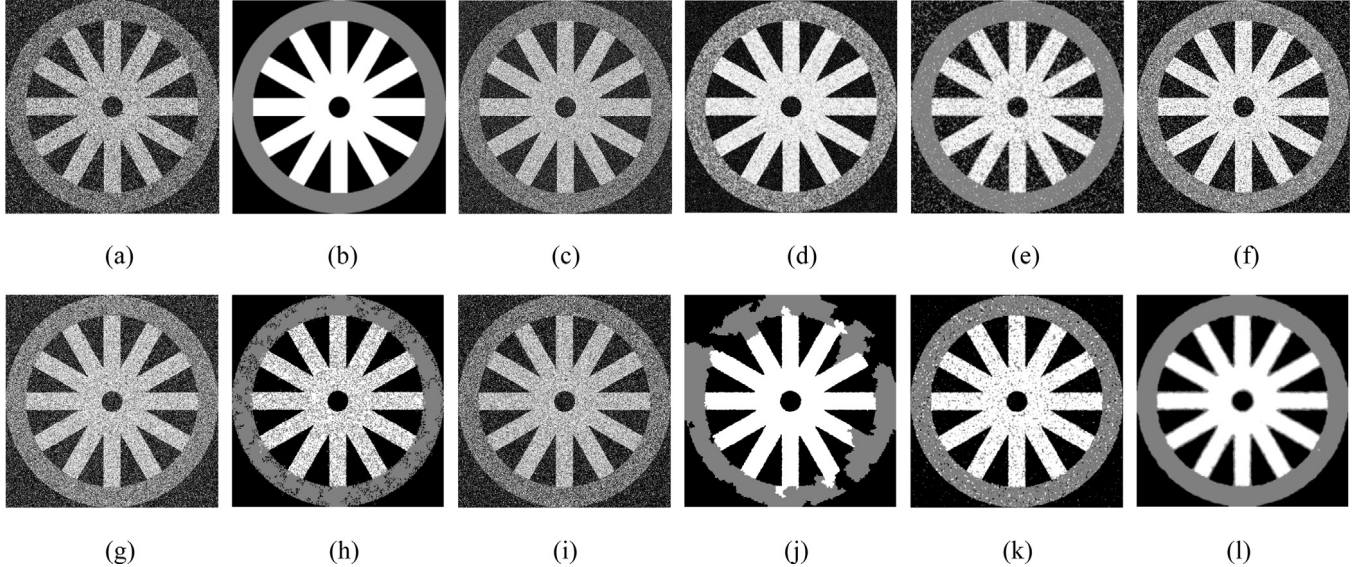


Fig. 3. Segmentation results on synthetic image 1 corrupted by 15% mixed noise using ten methods. (a) Original image with mixed noise. (b) Ground-truth. (c) FCM result. (d) FGFCM result with $\lambda_s = 3$ and $\lambda_g = 5$. (e) FLICM result. (f) ARKFCM result. (g) IIFCM result with $\lambda = 1.5$. (h) FRFCM result. (i) FLDNICM result. (j) SFFCM result. (k) APFCM_S result with $p = 3$, $q = 6$, $\alpha = 0.6$ and $\lambda = 10^7$. (l) FCM_SICM result with $\sigma_d = 5$ and $\sigma_r = 2$.

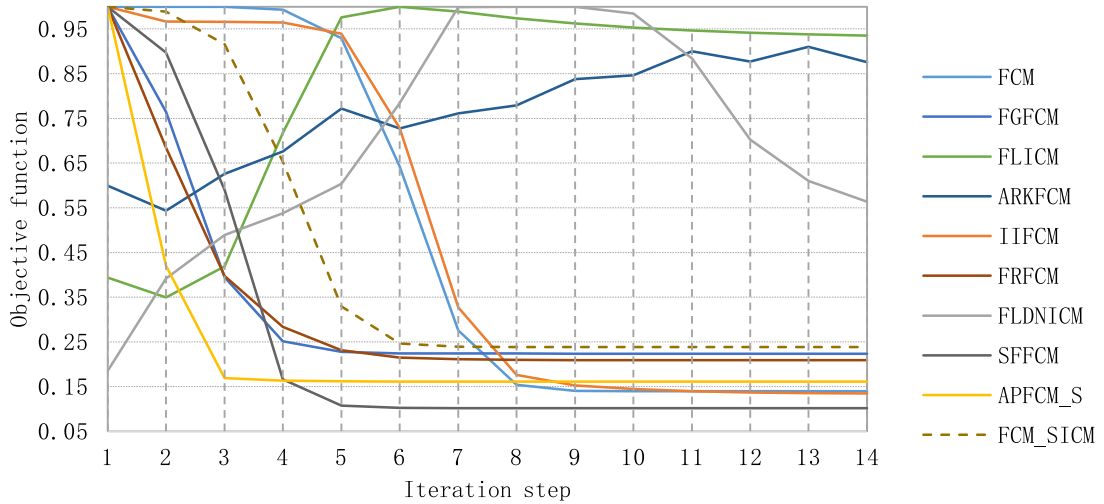


Fig. 4. Graph of objective function curves that normalized into [0, 1] of ten methods for Fig. 3.

where m and n are the height and width of the image respectively, $I_{GT}(x, y)$ and $I_{FM}(x, y)$ are the luminance of pixels located at (x, y) in the ground-truth and in the segmented result respectively, μ_{GT} and μ_{FM} are the global mean value of the ground-truth and of the segmented result respectively. It captures global statistics and local pixel matching information simultaneously [39]. The larger the E-Measure, the better the result is.

5.3. Parameter settings

For all the methods, set weighting exponent on membership degree $m = 2$, minimum error $\varepsilon = 0.001$ and the error between objective function values from last and previous iterations are used for stopping condition. For FGFCM, set neighborhood size of 9×9 . For FLICM, ARKFCM, FLDNICM, IIFCM, APFCM_S, set neighborhood size of 5×5 . For FRFCM, square structuring element size is 3×3 and membership median filtering window size is 5×5 . Every method is executed 10 times and the best results are shown. To segment noise corrupted images with different mixed noise, it is needed to select different parameters for each method

apparently. After the performance of plenty of experiments, parameters are chosen below. For FGFCM, the spatial scale factor and the grayscale level scale factor λ_s and λ_g are obtained in $[1.0, 10.0]$. For ARKFCM, weighted image filter is used. For IIFCM, spatial constraint λ is obtained in $[1.0, 5.0]$. For SFFCM, grayscale image is copied to the red, green and blue channel respectively to form a color image since SFFCM is designed to segment color image and set minimal SE $r_1 = 3$, minimal error threshold $\eta = 0.0001$ for MMGR-WT proposed in [22]. For APFCM_S, p , q and α are obtained in $[0.5, 6.0]$. For FCM_SICM, σ_d and σ_r are obtained in $[1.0, 7.0]$.

5.4. Results on grayscale images

The first experiment is to segment a fingerprint image (Fig. 1(a): 798×958 pixels) into two clusters, the second experiment is to segment synthetic image 1 that looks like a wheel (Fig. 3(a): 700×700 pixels, three classes with three grayscale levels taken as 0, 127, 255) and the third experiment is to segment synthetic image 2 (Fig. 5(a): 256×256 pixels, four

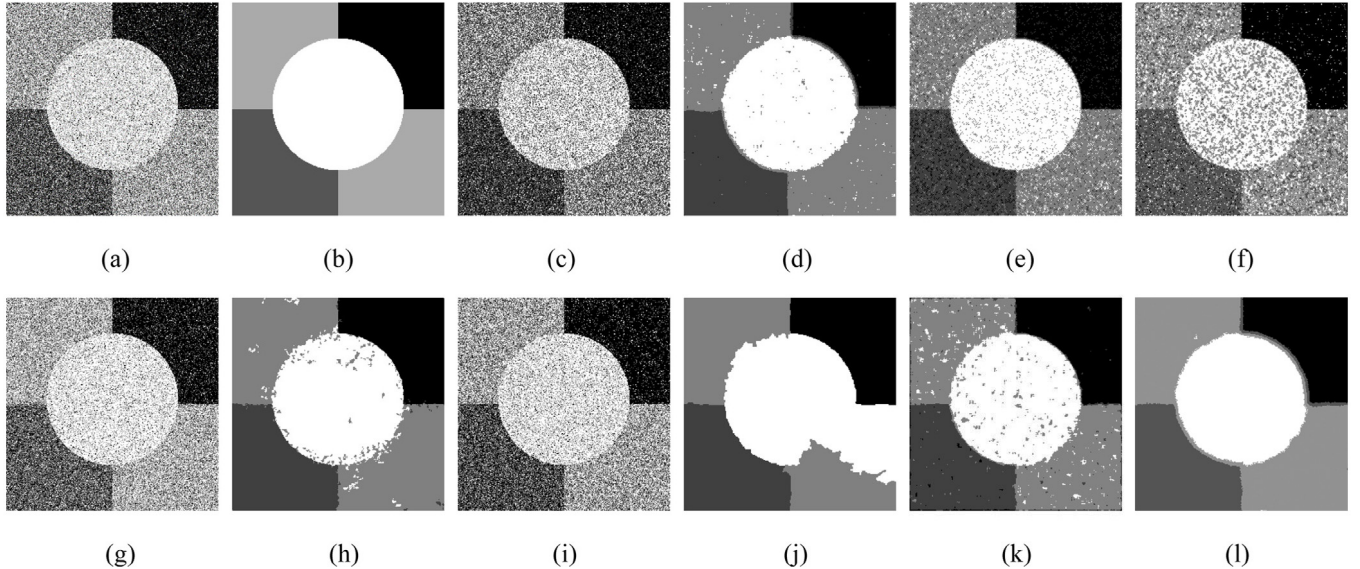


Fig. 5. Segmentation results on synthetic image 2 corrupted by 5% mixed noise using 10 methods. (a) Original image corrupted by 5% mixed noise. (b) Ground-truth. (c) FCM result. (d) FGFCM result with $\lambda_s = 3$ and $\lambda_g = 5$. (e) FLICM result. (f) ARKFCM result. (g) IIIFCM result with $\lambda = 1.5$. (h) FRFCM result. (i) FLDNICM result. (j) SFFCM result. (k) APFCM_S result with $p = 3$, $q = 6$, $\alpha = 0.6$ and $\lambda = 10^7$. (l) FCM_SICM result with $\sigma_d = 3.5$ and $\sigma_r = 2$.

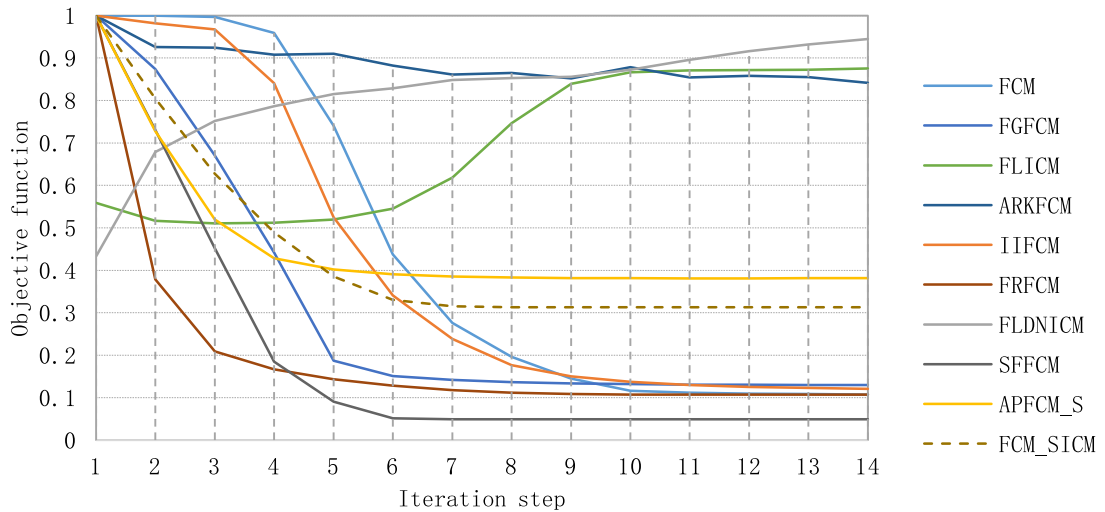


Fig. 6. Graph of objective function curves that normalized into [0, 1] of ten methods for Fig. 5.

classes with four grayscale levels taken as 0, 85, 170, 255). Visual and numerical results are shown in Figs. 1–6 and from Tables 1–4, respectively.

From Tables 1–3, it is noticed that all methods perform well when 1% mixed noise exists. As noise is more severe, performances of all methods are decreased and that of FCM, ARKFCM, IIFCM, SFFCM and FLDNICM are decreased quickly. Spatial information is utilized among all these methods except FCM, but uncertainty of images under mixed noise is way too high for kernel method in ARKFCM, intuitionistic fuzzy set in IIFCM, superpixel method in SFFCM and prior information function in FLDNICM. FGFCM, FLICM, FRFCM and APFCM_S are performed well to some extent due to local spatial and intensity information and shown in Figs. 1, 3 and 5, noise pixels in their results are less and gathered into bigger clusters. Compared with above methods, the proposed method uses fast bilateral filter and adaptive weights constraining not only the spatial and intensity information but also the original FCM. Noise pixels in the results are well reduced and the results are better than other methods

mentioned above. Comparisons in Table 4 shows that with the mixed noise becomes heavier, numbers of iteration steps are generally increased. It can be seen from Figs. 2, 4 and 6 that decreasing speeds of the objective functions of FGFCM, FRFCM, SFFCM and APFCM_S are fast while objective functions of FLICM, ARKFCM and FLDNICM are not obviously decreased. The numbers of iterations of FLICM, ARKFCM and APFCM_S are generally more than 100, though the objective function of APFCM_S decreases fast. Due to the membership linking, the number of iterations of FCM_SICM is well reduced compared with methods above.

After presenting the experiment results on grayscale images, rules for parameter selection for FCM_SICM are also be discussed.

For FCM_SICM, parameters of geometric spread σ_d and photometric spread σ_r are crucial to be required. The SA and mIoU results of Figs. 1(b) and 3(b) corrupted by mixed noise are shown in Fig. 7. From Fig. 7, it can be seen that with different σ_d and σ_r , FCM_SICM produces different segmentation results. Figs. 7(a) and 7(c) indicates that when $\sigma_d = 1$, SA and mIoU are not stable and not good enough. When σ_d increases, the changing trend of SA

Table 1

SA (%) comparisons of ten methods on three test images corrupted by different mixed noise.

Class	Mixed noise	FCM	FGFCM	FLICM	ARKFCM	IIFCM	FRFCM	FLDNICM	SFFCM	APFCM_S	FCM_SICM
Fingerprint image	1%	96.29	95.58	97.82	98.40	97.50	96.91	97.76	95.32	97.45	98.28
	5%	78.61	94.78	95.69	93.12	85.91	95.08	82.36	86.05	95.78	96.37
	10%	68.95	92.57	92.77	69.03	77.34	91.93	71.41	76.38	93.62	95.14
	15%	63.43	88.85	85.49	57.27	71.32	87.73	64.64	73.92	89.89	93.72
	20%	60.20	83.98	85.41	75.73	65.72	81.44	60.88	73.25	84.78	91.91
Synthetic image 1	1%	97.49	97.76	97.61	88.13	98.91	99.89	98.48	99.18	99.84	99.52
	5%	75.34	97.38	95.77	90.24	80.54	99.39	77.89	99.01	98.74	98.25
	10%	63.57	94.75	90.04	78.57	66.23	96.55	64.79	97.24	96.20	97.84
	15%	57.33	89.77	78.94	71.28	58.97	85.59	58.37	88.97	91.75	96.05
	20%	53.32	89.12	68.26	64.21	54.68	78.21	54.19	76.51	86.52	95.30
Synthetic image 2	1%	76.93	97.11	97.69	93.73	92.15	99.70	88.75	99.41	99.57	99.24
	5%	52.89	92.57	82.50	71.26	58.52	85.48	54.32	88.52	94.63	97.40
	10%	42.97	84.08	66.94	58.75	47.05	70.52	41.55	87.98	84.91	95.18
	15%	38.89	75.10	56.56	52.32	40.73	47.89	38.42	85.36	74.38	94.06
	20%	35.37	68.78	49.29	49.10	35.28	63.05	35.96	79.82	61.35	92.84

Table 2

mIoU (%) comparisons of ten methods on test images corrupted by different mixed noise.

Class	Mixed noise	FCM	FGFCM	FLICM	ARKFCM	IIFCM	FRFCM	FLDNICM	SFFCM	APFCM_S	FCM_SICM
Fingerprint image	1%	92.48	91.11	95.50	96.66	94.83	93.71	95.37	90.58	94.75	96.42
	5%	64.28	89.58	91.29	86.49	73.86	90.15	69.55	74.96	91.50	92.60
	10%	52.33	85.54	85.76	52.68	61.34	84.32	55.30	61.66	87.43	90.28
	15%	46.47	79.22	73.85	39.68	54.15	77.22	47.65	58.54	80.97	87.62
	20%	42.97	71.61	72.62	58.95	48.25	67.93	43.71	57.71	73.03	84.49
Synthetic image 1	1%	94.75	95.41	95.08	78.12	97.75	99.77	96.81	98.39	99.66	98.52
	5%	59.32	93.62	91.58	81.37	66.49	98.72	62.20	98.05	97.33	97.65
	10%	45.73	89.44	81.84	64.10	49.00	92.80	46.63	94.50	92.13	94.89
	15%	57.33	80.70	66.27	55.34	41.43	73.38	39.89	79.88	83.81	92.00
	20%	35.08	79.78	53.12	47.84	36.82	62.52	35.52	61.84	75.20	90.66
Synthetic image 2	1%	80.21	95.17	96.82	93.53	91.33	99.71	87.57	99.22	99.48	98.78
	5%	57.12	91.33	82.45	73.66	59.18	86.75	57.00	89.07	93.69	96.60
	10%	49.00	84.42	65.06	62.47	50.08	76.04	46.69	87.55	83.64	94.24
	15%	45.02	77.63	53.58	56.43	45.72	63.17	43.66	84.06	72.74	92.43
	20%	41.99	71.63	47.89	52.17	41.23	70.01	41.87	84.13	62.84	91.15

Table 3

E-measure (%) comparisons of ten methods on test images corrupted by different mixed noise.

Class	Mixed noise	FCM	FGFCM	FLICM	ARKFCM	IIFCM	FRFCM	FLDNICM	SFFCM	APFCM_S	FCM_SICM
Fingerprint image	1%	96.25	95.57	97.82	98.40	97.50	96.81	97.75	95.33	97.45	98.28
	5%	76.97	94.78	95.71	93.12	85.77	95.08	80.75	85.09	95.76	96.38
	10%	66.25	92.52	92.78	60.00	77.35	91.96	68.32	72.04	93.60	95.12
	15%	60.12	88.63	85.19	43.99	71.26	87.72	60.58	69.20	89.66	93.71
	20%	56.26	83.53	84.44	75.59	64.70	80.87	56.39	68.39	83.74	91.60

Table 4

Number of iteration steps of ten methods on three test images corrupted by different mixed noise.

Class	Mixed noise	FCM	FGFCM	FLICM	ARKFCM	IIFCM	FRFCM	FLDNICM	SFFCM	APFCM_S	FCM_SICM
Fingerprint image	1%	13	14	88	>100	18	13	18	10	>100	8
	5%	17	15	>100	>100	38	17	23	15	>100	8
	10%	16	17	>100	>100	42	20	22	14	>100	11
	15%	16	20	>100	>100	45	26	25	15	>100	13
	20%	16	24	>100	>100	36	31	23	16	>100	12
Synthetic image 1	1%	15	10	67	>100	30	10	18	9	>100	8
	5%	25	13	91	>100	41	15	35	10	>100	9
	10%	23	19	>100	>100	40	33	36	33	>100	9
	15%	20	28	>100	>100	34	32	29	26	>100	11
	20%	20	46	>100	>100	32	28	33	27	>100	13
Synthetic image 2	1%	27	11	49	>100	28	13	35	10	>100	9
	5%	28	17	>100	>100	23	32	38	13	>100	11
	10%	30	39	>100	>100	35	38	42	13	>100	11
	15%	24	84	>100	>100	32	34	31	18	>100	15
	20%	25	94	>100	>100	28	35	48	24	>100	20

and mIoU becomes stable with $\sigma_r > 2$. From Figs. 7(b) and 7(d), it is indicated that the changing trend of SA and mIoU are stable with $\sigma_r > 2$ when σ_d is specified. But a small σ_d with any σ_r are not suitable for FCM_SICM to produce a well-segmented result. Finally the conclusion is drawn. Firstly, FCM_SICM is relatively

insensitive to σ_r and thus the choice for σ_r is less important than the choice for σ_d . Here, $\sigma_r > 2$ is recommended. Secondly, when noise is severe, it is crucial to apply a large σ_d , like $\sigma_d = 4$ or 5 when 15% mixed noise exists, but not too large, otherwise an over-segmented result would be produced.

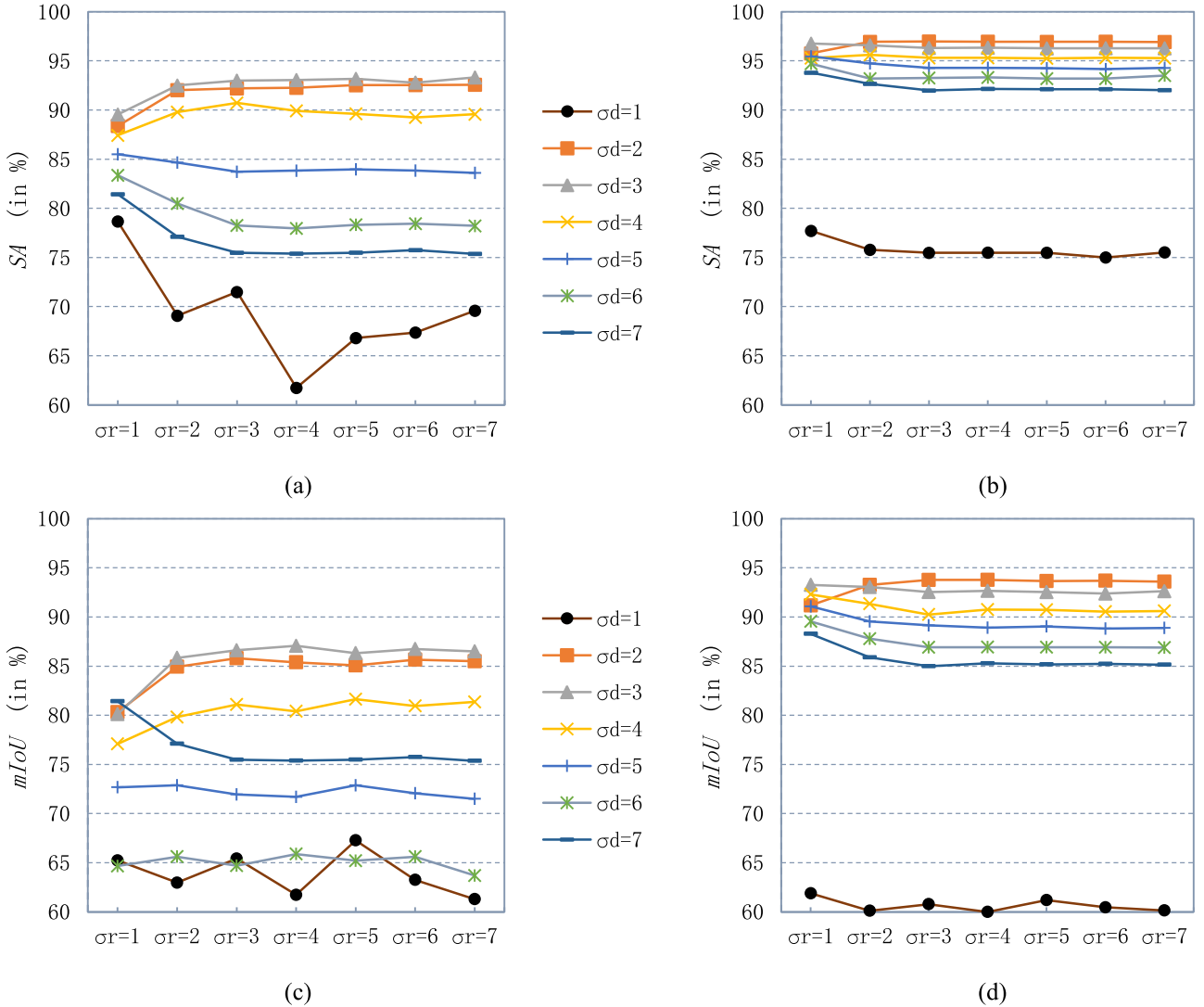


Fig. 7. SA and mIoU of Figs. 1(a) and 3(a) corrupted by mixed noise with different σ_d and σ_r using FCM_SICM. (a) SA of segmentation result of Fig. 1(a) corrupted by 15% mixed noise. (b) SA of segmentation result of Fig. 3(a) corrupted by 10% mixed noise. (c) mIoU of segmentation result of Fig. 1(a) corrupted by 15% mixed noise. (d) mIoU of segmentation result of Fig. 3(a) corrupted by 10% mixed noise.

5.5. Experiments on color images

Furthermore, segmentations on color images are shown in Figs. 8–11. Every segmentation result is the best result in 10 times of operation. In Figs. 9–10, in order to distinguish different segmentation areas, especially in results full of noise pixels, high contrast colors are used. Four color rectangles in Fig. 8(a), plane, cloud and sky in Fig. 9(a) and six images in the first row of Fig. 10 corrupted by mixed noise are tested among ten methods. Six images in Fig. 11 are tested using FCM_SICM.

In Figs. 8 and 9, due to high uncertainty of mixed noise, results of methods except for FRFCM, SFFCM and FCM_SICM are full of noise pixels. For FRFCM, morphological reconstruction is able to suppress most of the noise pixels in green region in Fig. 8(h) and in the whole area of Fig. 9(h), but there still exists some noise pixels in the rest regions. For SFFCM, MMGR-WT method, which is based on watershed method to generate superpixels and morphological reconstruction, is able to suppress all noise pixels, but watershed method can be misled by rest of noise pixels that morphological reconstruction cannot suppress. Therefore, mis-segmentation areas in Figs. 8(i) and 9(i) are appeared. In Fig. 10, FGFCM, FLICM SFFCM and FCM_SICM are able to remove most of

noise pixels but mis-segmentation exists. In Figs. 8–10, the results of FCM_SICM still perform well. In Fig. 11, FCM_SICM results of six images are well segmented and noise pixels are almost clear.

5.6. Comparison of computational overload

Computational overload is a key reference to evaluate methods. Generally, accurate computational complexity is very difficult to be acquired. Here, for clustering process, numbers of computational steps of objective functions are computed. Table 5 shows the number of computational steps and time complexities of ten methods, where T is the number of iteration steps, Q is the number of grayscale levels, S is the number of pixels in local window, T_F is the number of iteration steps of FCM as FLDNICM requires FCM to obtain the initial membership degrees, T_M is the number of iteration steps for MMGR-WT proposed in [22], N_W is the number of computational steps of watershed method, N_D and Q_D are the numbers of pixels and grayscale levels in downsampled image respectively.

In Table 5, for FCM_SICM, $N_D \times Q_D \times \log_2(N_D \times Q_D)$ is the number of computational steps of fast bilateral filter in [36]. From Table 5, it can be seen that local information is used either

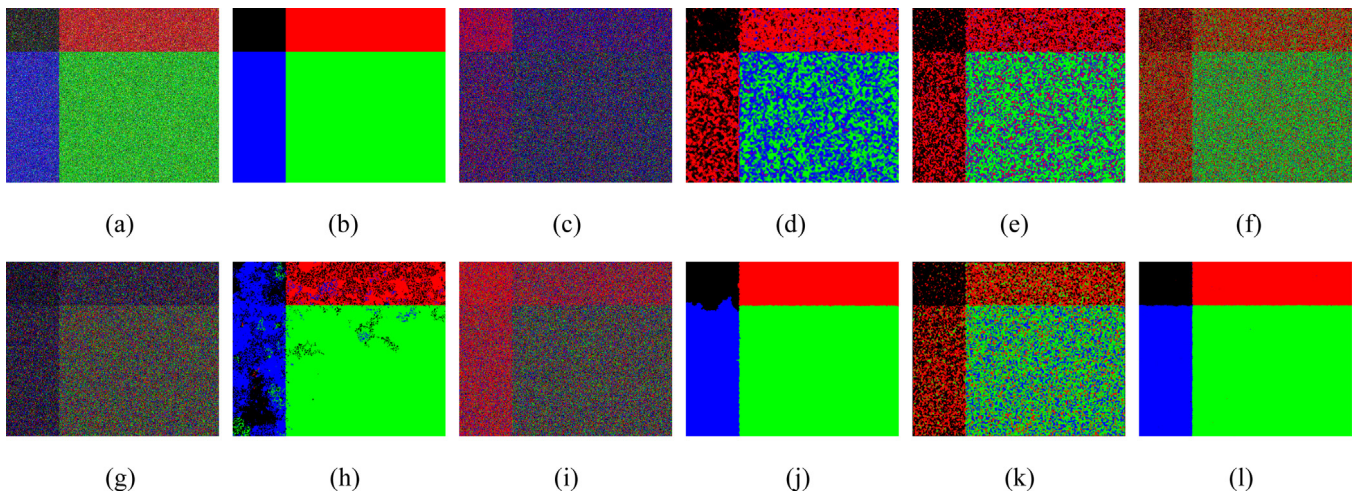


Fig. 8. Segmentation results on synthetic image 3 corrupted by 15% mixed noise using 10 methods. (a) Original image corrupted by 15% mixed noise. (b) Ground-truth. (c) FCM result. (d) FGFCM result with $\lambda_s = 10$ and $\lambda_g = 15$. (e) FLICM result. (f) ARKFCM result. (g) IIFCM result with $\lambda = 1.5$. (h) FRFCM result. (i) FLDNICM result. (j) SFFCM result. (k) APFCM_S result with $p = 3$, $q = 6$, $\alpha = 0.6$ and $\lambda = 10^8$. (l) FCM_SICM result with $\sigma_d = 5$ and $\sigma_r = 2.5$.

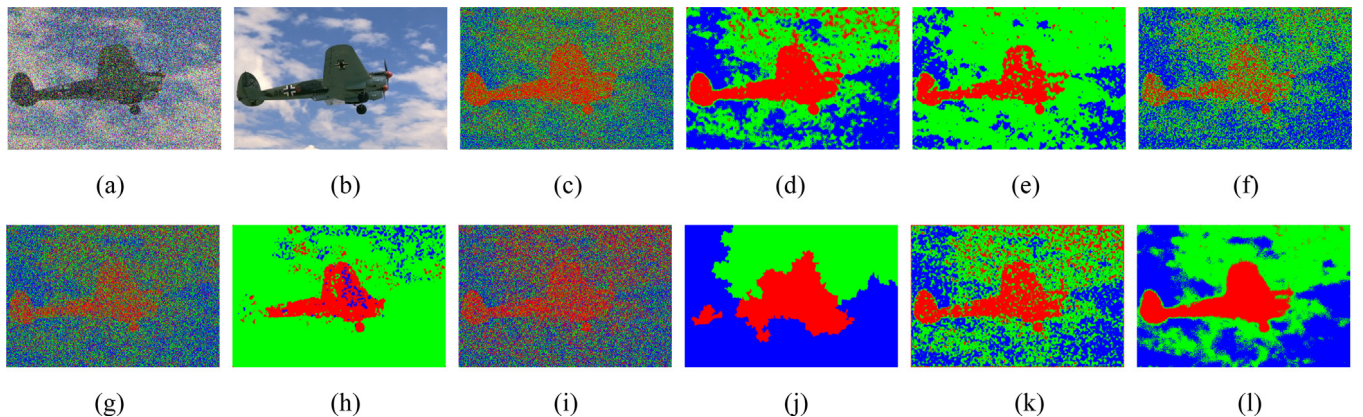


Fig. 9. Segmentation results on plane No.1 image corrupted by 15% mixed noise using 10 methods. (a) Original image corrupted by 15% mixed noise. (b) Original image without noise. (c) FCM result. (d) FGFCM result with $\lambda_s = 10$ and $\lambda_g = 15$. (e) FLICM result. (f) ARKFCM result. (g) IIFCM result with $\lambda = 1.5$. (h) FRFCM result. (i) FLDNICM result. (j) SFFCM result. (k) APFCM_S result with $p = 3$, $q = 6$, $\alpha = 0.6$ and $\lambda = 10^8$. (l) FCM_SICM result with $\sigma_d = 5$ and $\sigma_r = 2.5$.

Table 5
Complexity overloads of ten methods.

Methods	Numbers of computational steps	Time complexity
FCM	$N \times K \times T$	$O(n^3)$
FGFCM	$N \times S + Q \times K \times T$	$O(n^3)$
FLICM	$N \times K \times S \times T$	$O(n^4)$
ARKFCM	$N \times S \times (S - 1) + N \times K \times T$	$O(n^3)$
IIFCM	$N + N \times K \times S \times T$	$O(n^4)$
FRFCM	$N \times S + Q \times K \times T$	$O(n^3)$
FLDNICM	$N \times K \times T_F + N \times S + N \times K \times S \times T$	$O(n^4)$
SFFCM	$N \times S \times T_M + N_w + Q \times K \times T$	$O(n^3)$
APFCM_S	$N \times S + N \times K \times S \times T$	$O(n^4)$
FCM_SICM	$N_D \times Q_D \times \log_2(N_D \times Q_D) + N + (N + N) \times K \times T$	$O(n^3)$

before clustering or during clustering. For methods using local information during clustering including FLICM, IIFCM, FLDNICM, APFCM_S, time complexities are $O(n^4)$ and thus require much time to run. However, for methods including FGFCM, ARKFCM, FRFCM, SFFCM and FCM_SICM, there is no local information used during clustering and therefore running time can be reduced.

6. Discussion

In this section, advantages and disadvantages of FCM_SICM are discussed compared with methods in [5,10–25]. Firstly, for histogram clustering methods, clustering speed is very fast, which is the most obvious advantage that FCM_SICM cannot reach. However, histogram only contains intensity information and thus the results are not satisfied compared with that of FCM_SICM. Secondly, for methods using prior probability function, the advantage is that suitable prior knowledge can not only lead the method to segment well but also reduce instability caused by random initialization. Without prior information, FCM_SICM can be unstable sometimes (result qualities are varied). However, the uncertainty of noise images is high and thus it is hard to obtain appropriate prior knowledge. Thirdly, for methods using kernel methods, non-linear classification ability is suitable for more diversely distributed datasets while FCM_SICM is not. However, experimental results prove that for noise images, kernel methods are limited. Next, for methods using spatial and intensity information, it can be seen from the results that noise pixels are well treated to some extent when noise is light. But with noise becomes more severe, bigger local window is required and

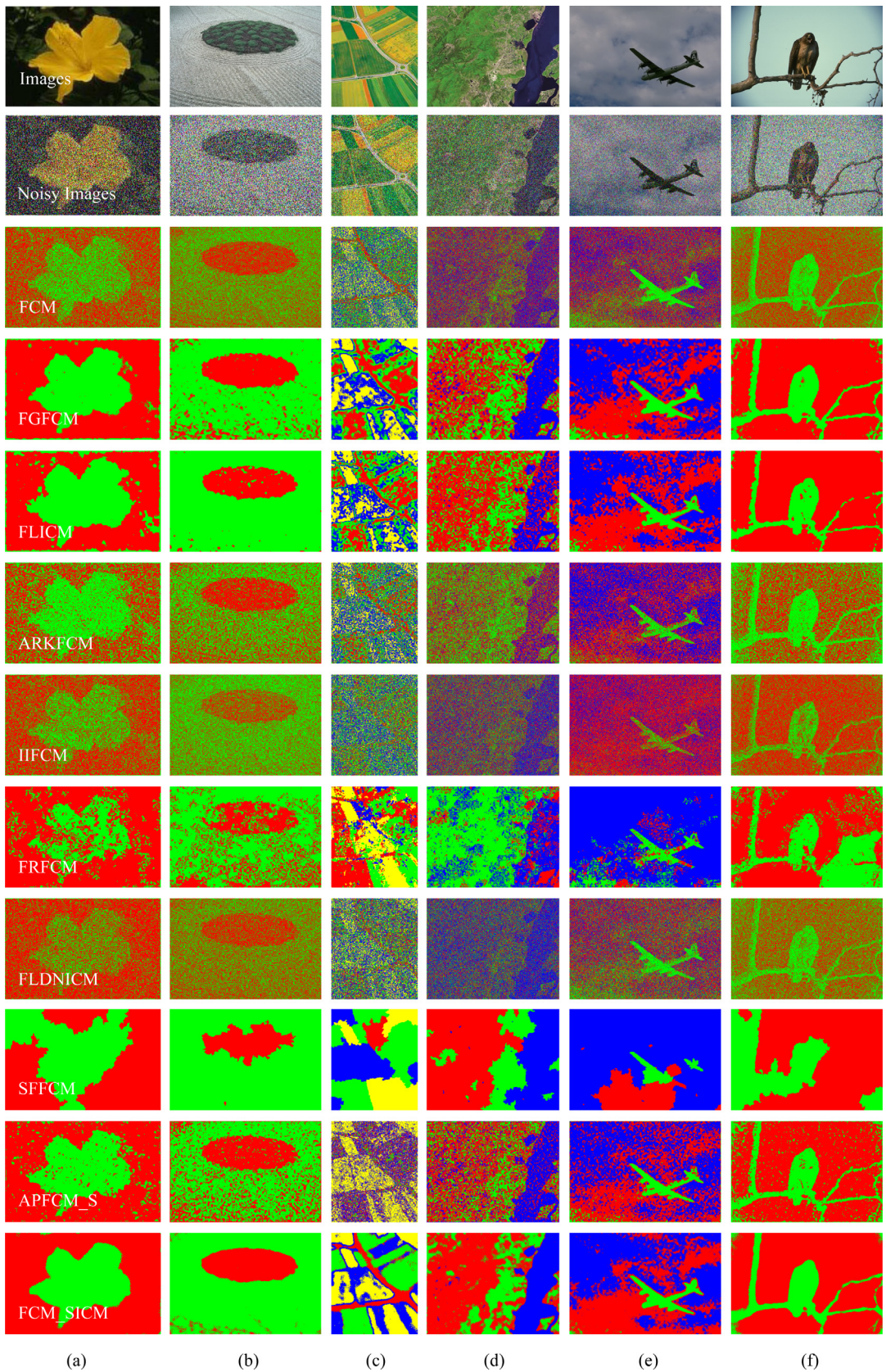


Fig. 10. Results of mixed noise corrupted color images. (a)-(f) are results of ten methods. (a) Result on “yellow flower” image corrupted by 15% mixed noise with $\sigma_d = 5$ and $\sigma_r = 2$ for FCM_SICM. (b) Result on “parterre” image corrupted by 15% mixed noise with $\sigma_d = 5$ and $\sigma_r = 2$ for FCM_SICM. (c) Result on “road and field” image corrupted by 5% mixed noise with $\sigma_d = 4$ and $\sigma_r = 2$ for FCM_SICM. (d) Result on remote sensing image corrupted by 15% mixed noise with $\sigma_d = 5$ and $\sigma_r = 2$ for FCM_SICM. (e) Result on “plane No. 2” image corrupted by 5% mixed noise with $\sigma_d = 4$ and $\sigma_r = 2$ for FCM_SICM. (f) Result on “eagle” image corrupted by 15% mixed noise with $\sigma_d = 4$ and $\sigma_r = 2$ for FCM_SICM.

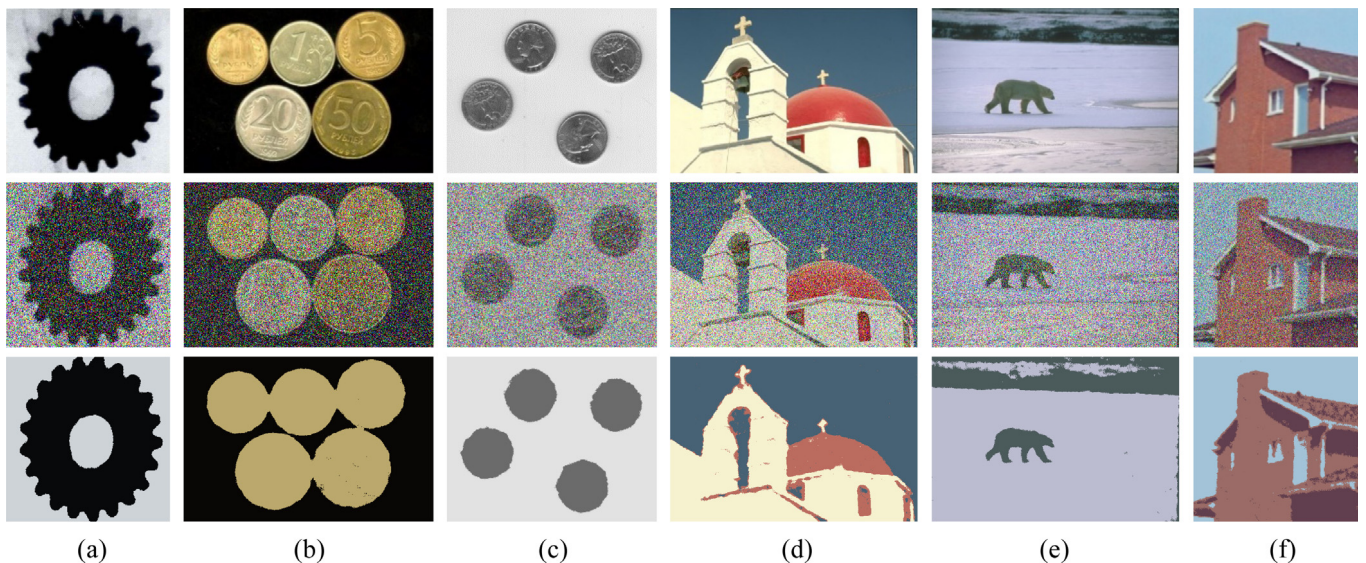


Fig. 11. Results of FCM_SICM. (a) Result of “gear” image corrupted by 20% mixed noise with $\sigma_d = 5$ and $\sigma_r = 2$. (b) Result of “five coins” image corrupted by 20% mixed noise with $\sigma_d = 5$ and $\sigma_r = 2$. (c) Result of “four coins” image corrupted by 20% mixed noise with $\sigma_d = 5$ and $\sigma_r = 2$. (d) Result of “roof” image corrupted by 10% mixed noise with $\sigma_d = 4$ and $\sigma_r = 2$. (e) Result of “polar bear” image corrupted by 10% mixed noise with $\sigma_d = 3$ and $\sigma_r = 4$. (f) Result of “house” image corrupted by 10% mixed noise with $\sigma_d = 4$ and $\sigma_r = 2$.

number of iteration steps is increased and meanwhile qualities of segmentation results are not satisfied compared with FCM_SICM.

7. Conclusion

For noise image segmentation problem using FCM, the key issue is that local information is not used. In order to provide a better solution for noise image segmentation, an improved FCM method with adaptive spatial & intensity constraint and membership linking (FCM_SICM) is presented. Firstly, local spatial and intensity information is considered via fast bilateral filter before clustering process, which is able to reduce time complexity of objective function from $O(n^4)$ to $O(n^3)$. Secondly, considering that control of influence of original FCM in objective function is not supposed to be ignored, a new constraining way is introduced. When noise exists, it is supposed to reduce and increase the influences of the original FCM and the spatial & intensity information respectively. Multiplied by a constant number, reciprocal of the difference image and the difference image itself are used as constraints to constrain the original FCM and the spatial & intensity information. Finally, in order to reduce the number of iteration steps, membership linking is introduced by firstly summing all membership degrees calculated from previous iteration within every cluster in squared logarithmic form and then putting it in the denominator place in objective function. Experiments are performed using FCM, FGFCM, FLICM, ARKFCM, IIFCM, FRFCM, FLDNICM, SFFCM, APFCM_S and the proposed method FCM_SICM under mixed noise. Results show that FCM_SICM outperforms other methods as noise becomes severe, the number of iterations remains the least and time complexity is not increased, which further prove that FCM_SICM is effective in handling noise image segmentation problem. Additionally, advantages and disadvantages of FCM_SICM and other recent methods are discussed, which presents a better view for recent FCM variants.

However, there are still some aspects deserve further research: (1) The selection of proper σ_d and σ_r for local spatial information and local intensity information is still an open problem. In experience, the more severe the noise, the larger the σ_d , and $\sigma_r = 2$ or 3 is enough in most of time. How to reduce manual load is a challenge. (2) Additive noise image segmentation is studied

through years and many FCM variants yield good performance. However, additive noise is not the only noise type and single noise or combination of two noise types is sometimes ideal in real environment. Although in this paper, mixed noise including multiplicative noise is added into the experiments, how to treat multiplicative noise or mixed noise including more noise types is deserved further research.

Declaration of competing interest

The authors declare that they have no known competing financial interests or personal relationships that could have appeared to influence the work reported in this paper.

CRediT authorship contribution statement

Qingsheng Wang: Conceptualization, Methodology, Software, Validation, Formal analysis, Data curation, Investigation, Writing - original draft, Visualization. **Xiaopeng Wang:** Resources, Writing - review & editing, Supervision, Project administration, Funding acquisition. **Chao Fang:** Writing - review & editing. **Wenting Yang:** Writing - review & editing.

Acknowledgments

The authors are very pleased to show appreciation to the anonymous reviewers for their comments and constructive suggestions. This work was supported by the National Natural Science Foundation of China under Grant 61761027.

References

- [1] N.R. Pal, S.K. Pal, A review on image segmentation techniques, *Pattern Recognit.* 26 (9) (1993) 1277–1294, [http://dx.doi.org/10.1016/0031-3203\(93\)90135-J](http://dx.doi.org/10.1016/0031-3203(93)90135-J).
- [2] X. Muñoz, J. Freixenet, X. Cufí, J. Martí, Strategies for image segmentation combining region and boundary information, *Pattern Recogn. Lett.* 24 (1) (2003) 375–392, [http://dx.doi.org/10.1016/S0167-8655\(02\)00262-3](http://dx.doi.org/10.1016/S0167-8655(02)00262-3).
- [3] P.A. Khaire, N.V. Thakur, An overview of image segmentation algorithms, *Int. J. Image Process. Vis. Sci.* 1 (2) (2012) 62–68.
- [4] S. Jain, V. Laxmi, Color image segmentation techniques: A survey, in: Proceedings of the International Conference on Microelectronics, Computing & Communication Systems, 2018, pp. 189–197.

- [5] S. Krinidis, V. Chatzis, A robust fuzzy local information c-means clustering method, *IEEE Trans. Image Process.* 19 (5) (2010) 1328–1337, <http://dx.doi.org/10.1109/TIP.2010.2040763>.
- [6] W.S. Sarle, Methods for clustering data, *Technometrics* 32 (2) (1990) 227–229, <http://dx.doi.org/10.1080/00401706.1990.10484648>.
- [7] S. Wazarkar, B.N. Keshavamurthy, A survey on image data analysis through clustering technique-s for real world applications, *J. Vis. Commun. Image Represent.* 55 (2018) 596–626, <http://dx.doi.org/10.1016/j.jvcir.2018.07.009>.
- [8] L.A. Zadeh, Fuzzy sets, *Inf. Control* 8 (1965) 338–435, [http://dx.doi.org/10.1016/S0019-9958\(65\)90241-X](http://dx.doi.org/10.1016/S0019-9958(65)90241-X).
- [9] C. Feng, D. Zhao, Segmentation of longitudinal brain MR images using bias correction embedded fuzzy c-means with non-locally spatio-temporal regularization, *J. Vis. Commun. Image Represent.* 38 (2016) 517–529, <http://dx.doi.org/10.1016/j.jvcir.2016.03.027>.
- [10] S. Chen, D. Zhang, Robust image segmentation using FCM with spatial constraints based on new kernel-induced distance measure, *IEEE Trans. Syst. Man. Cybern.* 34 (4) (2004) 1907–1916, <http://dx.doi.org/10.1109/TSMCB.2004.831165>.
- [11] W. Cai, S. Chen, D. Zhang, Fast and robust fuzzy c-means clustering method incorporating lo-cal information for image segme-nation, *Pattern Recognit.* 40 (3) (2007) 825–838, <http://dx.doi.org/10.1016/j.patcog.2006.07.011>.
- [12] S.P. Chatzis, T.A. Varvarigou, A fuzzy clustering approach toward hidden markov random field models for enhanced spatially constrained image segmentation, *IEEE Trans. Fuzzy Syst.* 16 (5) (2008) 1351–1361, <http://dx.doi.org/10.1109/TFUZZ.2008.2005008>.
- [13] M. Gong, Y. Liang, J. Shi, W. Ma, J. Ma, Fuzzy c-means clustering with local information and kernel metric for image segm-entation, *IEEE Trans. Image Process.* 22 (2) (2013) 573–584, <http://dx.doi.org/10.1109/TIP.2012.2219547>.
- [14] A. Elazab, C. Wang, F. Jia, J. Wu, G. Li, Q. Hu, Segmentation of brain tissues from magnetic resonance images using adaptiv-ely regularized kernel-based fuzzy c-means clustering, *Comput. Math. Methods Med.* (2015) <http://dx.doi.org/10.1155/2015/485495>.
- [15] G. Liu, Y. Zhang, A. Wang, Incorporating adaptive local information into fuzzy clustering for image segmentation, *IEEE Trans. Image Process.* 24 (11) (2015) 3990–4000, <http://dx.doi.org/10.1109/TIP.2015.2456505>.
- [16] H. Barrah, A. Cherkaoui, D. Sarsri, Robust FCM algorithm with local and gray information for image segmentation, *Adv. Fuzzy Syst.* (2016) 1–10, <http://dx.doi.org/10.1155/2016/6238295>.
- [17] H. Verma, R.K. Agrawal, A. Sharan, An improved intuitionistic fuzzy c-means clustering method incorporating local information for brain image segmentation, *Appl. Soft Comput.* 46 (2015) 543–557, <http://dx.doi.org/10.1016/j.asoc.2015.12.022>.
- [18] K.H. Memon, D. Lee, Generalised kernel weighted fuzzy c-means clustering algorithm with local information, *Fuzzy Sets and Systems* 340 (2018) 91–108, <http://dx.doi.org/10.1016/j.fss.2018.01.019>.
- [19] H. Zhang, L. Bruzzone, W. Shi, M. Hao, Y. Wang, Enhanced spatially constrained remotely sensed imagery classification using a fuzzy local double neighborhood information c-means clustering algorithm, *IEEE J. Sel. Top. Appl. Earth Obs. Remote Sens.* 11 (8) (2018) 2896–2910, <http://dx.doi.org/10.1109/JSTARS.2018.2846603>.
- [20] T. Lei, X. Jia, Y. Zhang, L. He, H. Meng, A.K. Nandi, Significantly fast and robust fuzzy c-means clustering method based on morphological reconstruction and membership filtering, *IEEE Trans. Fuzzy Syst.* 26 (5) (2018) 3027–3041, <http://dx.doi.org/10.1109/TFUZZ.2018.2796074>.
- [21] W. Zhang, X. Guo, T. Huang, J. Liu, J. Chen, Kernel-based robust bias-correction fuzzy weighted c-ordered means clustering a-lgorithm, *Symmetry* 11 (6) (2019) 753, <http://dx.doi.org/10.3390/sym11060753>.
- [22] T. Lei, X. Jia, Y. Zhang, L. He, H. Meng, A.K. Nandi, Superpixel-based fast fuzzy c-means for color image segmentation, *IEEE Trans. Fuzzy Syst.* 27 (9) (2019) 1753–1766, <http://dx.doi.org/10.1109/TFUZZ.2018.2889018>.
- [23] A. Halder, N.A. Talukdar, Robust brain magnetic resonance image segmentation using modified rough-fuzzy c-means with spatial constraints, *Appl. Soft Comput.* 85 (2019) 1–17, <http://dx.doi.org/10.1016/j.asoc.2019.105758>.
- [24] C. Feng, W. Li, J. Hu, K. Yu, D. Zhao, BCEFCM_S: Bias correction embedded fuzzy c-means with spatial constraint to segment multiple spectral images with intensity inhomogeneities and noises, *Signal Process.* 168 (2020) 1–21, <http://dx.doi.org/10.1016/j.sigpro.2019.107347>.
- [25] C. Wu, Y. Chen, Adaptive entropy weighted picture fuzzy clustering algorithm with spatial information for image segmentation, *Appl. Soft Comput.* 86 (2020) 1–23, <http://dx.doi.org/10.1016/j.asoc.2019.105888>.
- [26] K.S. Tan, N.A.M. Isa, Color image segmentation using histogram thresholding - fuzzy c-means hybrid approach, *Pattern Recognit.* 44 (2011) 1–15, <http://dx.doi.org/10.1016/j.patcog.2010.07.013>.
- [27] I.J. Sledge, T.C. Havens, J.M. Huband, J.C. Bezdek, J.M. Keller, Finding the number of clusters in ordered dissimilarities, *Soft Comput.* 13 (12) (2009) 1125–1142, <http://dx.doi.org/10.1007/s00500-009-0421-5>.
- [28] A. Kolesnikov, E. Trichina, T. Kauranne, Estimating the number of clusters in a numerical data set via quantization error modeling, *Pattern Recognit.* 48 (2015) 941–952, <http://dx.doi.org/10.1016/j.patcog.2014.09.017>.
- [29] A. Srivastava, M. Baranwal, S. Salapaka, On the persistence of clustering solutions and true number of clusters in a dataset, in: 33th AAAI Conference on Artificial Intelligence, 2019, <http://dx.doi.org/10.1609/aaai.v33i01.33015000>.
- [30] C. Patil, I. Baidari, Estimating the optimal number of clusters k in a dataset using data depth, *Data Sci. Eng.* 4 (2019) 132–140, <http://dx.doi.org/10.1007/s41019-019-0091-y>.
- [31] T. Calinski, J. Harabasz, A dendrite method for cluster analysis, *Commun. Stat.* 3 (1974) 1–27, <http://dx.doi.org/10.1080/03610927408827101>.
- [32] W.J. Krzanowski, Y.T. Lai, A criterion for determining the number of groups in a data set using sum-of-squares clustering, *Biometric* 44 (1988) 23–34, <http://dx.doi.org/10.2307/2531893>.
- [33] P.J. Rousseeuw, Silhouettes: A graphical aid to the interpretation and validation of cluster analysis, *J. Comput. Appl. Math.* 20 (1987) 53–65, [http://dx.doi.org/10.1016/0377-0427\(87\)90125-7](http://dx.doi.org/10.1016/0377-0427(87)90125-7).
- [34] R. Tibshirani, G. Walther, T. Hastie, Estimating the number of clusters in a data set via the gap statistic, *J. R. Stat. Soc. B* 63 (2) (2001) 411–423, <http://dx.doi.org/10.2307/2680607>.
- [35] C. Tomasi, R. Manduchi, Bilateral filtering for grayscale and color image, in: 6th IEEE International Conference on Computer Vision, 1998, pp. 839–846, <http://dx.doi.org/10.1109/ICCV.1998.710815>.
- [36] S. Paris, F. Durand, A fast approximation of the bilateral filter using a signal processing approach, *Int. J. Comput. Vis.* 81 (1) (2009) 24–52, <http://dx.doi.org/10.1007/s11263-007-0110-8>.
- [37] J.C. Dunn, A fuzzy relative of the ISODATA process and its use in detecting compact well separated clusters, *J. Cybern.* 3 (3) (1974) 32–57, <http://dx.doi.org/10.1080/01969727308546046>.
- [38] J.C. Bezdek, *Pattern Recognition with Fuzzy Objective Function Method*, Plenum Press, New York, 1981, <http://dx.doi.org/10.1007/978-1-4757-0450-1>.
- [39] D. Fan, C. Gong, Y. Cao, B. Ren, M. Cheng, A. Borji, Enhanced-alignment measure for binary foreground map evaluation, in: 27th International Joint Conference on Artificial Intelligence, 2018, pp. 698–704, <http://dx.doi.org/10.24963/ijcai.2018/97>.



Qingsheng Wang (1995-) is currently studying for his Master's degree at the School of Electronic and Information Engineering, Lanzhou Jiaotong University. His research interest is computer vision. wqshmzh521@hotmail.com



Xiaopeng Wang (1969-) is currently a professor of School of Electronic and Information Engineering, Lanzhou Jiaotong University. He received his Ph.D degree in signal and information processing from Northwestern Polytechnical University, China, in 2005. His interested research fields are image analysis and recognition. wangxiaopeng@mail.lzjtu.cn